

**CALIPSO surface
type effect on aerosol
type**

T. Kanitz et al.

This discussion paper is/has been under review for the journal Atmospheric Measurement Techniques (AMT). Please refer to the corresponding final paper in AMT if available.

Surface matters: limitations of CALIPSO V3 aerosol typing in coastal regions

**T. Kanitz¹, A. Ansmann¹, A. Foth², P. Seifert¹, U. Wandinger¹, R. Engelmann¹,
H. Baars¹, D. Althausen¹, C. Casiccia³, and F. Zamorano³**

¹Leibniz Institute for Tropospheric Research, Permoserstr. 15, 04318 Leipzig, Germany

²Leipzig Institute for Meteorology, University of Leipzig, Stephanstr. 3,
04103 Leipzig, Germany

³Ozone and RUV Laboratory, Universidad de Magallanes, Punta Arenas, 6210427, Chile

Received: 29 December 2013 – Accepted: 21 January 2014 – Published: 11 February 2014

Correspondence to: T. Kanitz (kanitz@tropos.de)

Published by Copernicus Publications on behalf of the European Geosciences Union.

Title Page

Abstract

Introduction

Conclusions

References

Tables

Figures

⏪

⏩

◀

▶

Back

Close

Full Screen / Esc

Printer-friendly Version

Interactive Discussion



Abstract

In the CALIPSO data analysis the surface type (land/ocean) is used to augment the aerosol characterization. However, this surface-dependent aerosol typing prohibits a correct classification of sea-breeze-related marine aerosol over land. This might result in a systematic overestimation of the particle extinction coefficient and of the aerosol optical thickness (AOT) of up to a factor of 3.5 over land in coastal areas. We present a long-term comparison of CALIPSO and ground-based lidar observations of the aerosol conditions in the coastal environment of southern Latin America (Punta Arenas, Chile, 53° S), performed in December 2009–April 2010. Punta Arenas is almost entirely influenced by marine particles throughout the year, indicated by a rather low AOT of 0.02–0.04. However, we found an unexpectedly high fraction of continental aerosol in the aerosol types inferred by means of CALIOP observations and, correspondingly, too high particle extinction values. Similar features of the CALIOP data analysis are presented for four other coastal areas around the world. Since CALIOP data serve as important input for global climate models, the influence of this systematic error was estimated by means of simplified radiative-transfer calculations.

1 Introduction

The spaceborne Cloud-Aerosol Lidar with Orthogonal Polarization (CALIOP, Winker et al., 2009) has acquired a unique, global vertically resolved data set on aerosols and clouds within the framework of the Cloud-Aerosol Lidar Infrared Pathfinder Satellite Observation (CALIPSO) mission since 2006. Among the great successes of CALIPSO are, e.g., the first documentation of the global vertical distribution of atmospheric dust as presented by Liu et al. (2008) and a product for further height-resolved simulations of the aerosol radiative effect on the Earth's radiation budget (Huang et al., 2009).

Since the beginning strong effort was put in the validation of the CALIOP observations. The vertical aerosol distribution as derived with CALIOP agrees well with

AMTD

7, 1333–1365, 2014

CALIPSO surface type effect on aerosol type

T. Kanitz et al.

Title Page

Abstract

Introduction

Conclusions

References

Tables

Figures

◀

▶

◀

▶

Back

Close

Full Screen / Esc

Printer-friendly Version

Interactive Discussion



CALIPSO surface type effect on aerosol type

T. Kanitz et al.

[Title Page](#)

[Abstract](#)

[Introduction](#)

[Conclusions](#)

[References](#)

[Tables](#)

[Figures](#)

[⏪](#)

[⏩](#)

[◀](#)

[▶](#)

[Back](#)

[Close](#)

[Full Screen / Esc](#)

[Printer-friendly Version](#)

[Interactive Discussion](#)



ground-based and airborne lidar observations (e.g., Mamouri et al., 2009; Pappalardo et al., 2010; Rogers et al., 2011). The aerosol optical thickness (AOT) of dust plumes as derived with CALIOP and in the framework of Aerosol Robotic Network (AERONET) showed good agreement in the Mediterranean (Schuster et al., 2012). However, discrepancies in the extinction coefficient were reported especially for Saharan mineral dust (Wandinger et al., 2010; Tesche et al., 2013) caused by an underestimated extinction-to-backscatter ratio (S_p) for Saharan dust, which has to be assumed in the CALIOP data algorithm to determine the particle extinction coefficient (Young and Vaughan, 2009; Young et al., 2013).

In the general data analysis of CALIOP, observed atmospheric layers are determined with a selective, iterated boundary location algorithm (Vaughan et al., 2009). The defined atmospheric layers are further categorized as cloud or aerosol layer (Liu et al., 2009). In the case of an aerosol layer a suitable S_p has to be found to determine the particle extinction coefficient. Therefore a following algorithm is based on a yes/no-decision tree with regard to the aerosol-layer-integrated backscatter coefficient, the approximated particle linear depolarization ratio, and the altitude of the aerosol layer. In addition, the surface type information (water/land) below the footprint of CALIOP is used in the aerosol type identification. The possible aerosol types are clean marine (with $S_p = 20$ sr at 532 nm), clean continental ($S_p = 35$ sr), pure dust ($S_p = 40$ sr), polluted dust ($S_p = 55$ sr), polluted continental ($S_p = 70$ sr), and smoke ($S_p = 70$ sr) (Omar et al., 2009; Lopes et al., 2013).

The aerosol typing of CALIOP was validated within various studies. For example, Burton et al. (2013) compared the aerosol typing of the backscatter lidar CALIOP with an airborne advanced high-spectral resolution lidar. In coastal regions, the authors found a bias towards too low extinction values in the CALIPSO data over water, because the CALIPSO data algorithm determined clean marine aerosol although terrestrial aerosol was transported to the sea and increased the absorptivity of the marine boundary layer. Such findings were also reported in the framework of ground-based

investigations (Schuster et al., 2012; Bridhikitti et al., 2013; Omar et al., 2013) and synergistic satellite observations (Oo and Holz, 2011).

Here, we report on another aspect of the CALIOP data analysis in coastal regions. Clean marine aerosol is only permitted over water surfaces (Omar et al., 2009). Hence, when CALIPSO crosses a coastal line (from sea to land), the S_p value immediately changes from 20 sr to 70 sr in the worst case, a jump from clean marine to smoke or polluted continental aerosol in the typing scheme. Correspondingly, abrupt changes in the particle extinction coefficients by a factor of up to 3.5 can occur, as will be shown below. Thus, an overestimation of the particle extinction coefficients over land within the sea breeze zone (≈ 100 km onshore, Miller et al., 2003) must be taken into account when studying aerosol conditions in coastal areas. This applies to the extinction coefficient in the CALIOP level2 data and vice versa to CALIOP level3 products. Consequently, it could explain the positive bias between CALIOP level3 AOT data and Sun-photometer-derived AOT at coastal sites, which was shown in Winker et al. (2013).

In the present study, ground-based lidar observations of Polly^{XT} (Althausen et al., 2009) conducted during a four-month campaign at Punta Arenas and data sets of CALIOP lidar and AERONET photometer observations were used to establish an aerosol climatology for the region around Punta Arenas, the most southern tail of Latin America. These measurements offered an excellent opportunity to validate CALIOP aerosol observations in the complex orography of the highly structured coastal environment with fast changes between water and land surfaces in the very south of Latin America. In the same latitudinal belt the first Aerosol Characterization Experiment was performed to determine aerosol background conditions for later investigation (Bates et al., 1998). Continental aerosol sources are limited to minimum and simple, almost pure marine conditions with rather low AOT values can be assumed around Punta Arenas so that any bias in the CALIPSO data analysis sensitively shows up and can be identified.

An introduction to the campaign at Punta Arenas is given at the beginning of Sect. 2. Afterwards, the instruments are briefly explained. In Sect. 3.1, we discuss a case study

CALIPSO surface type effect on aerosol type

T. Kanitz et al.

Title Page

Abstract

Introduction

Conclusions

References

Tables

Figures

⏪

⏩

◀

▶

Back

Close

Full Screen / Esc

Printer-friendly Version

Interactive Discussion



CALIPSO surface type effect on aerosol type

T. Kanitz et al.

Title Page

Abstract

Introduction

Conclusions

References

Tables

Figures



Back

Close

Full Screen / Esc

Printer-friendly Version

Interactive Discussion



of collocated measurements with Polly^{XT} and CALIOP in the area of Punta Arenas. Clear evidence of a misclassified aerosol layer within the CALIOP aerosol typing due to changes in the underlying surface type is presented. A larger set of observations from CALIOP is contrasted to combined Polly^{XT} and AERONET Sun Photometer measurements in Sect. 3.2 to evaluate the influence of the underlying surface on the aerosol climatology from CALIOP for the area of Punta Arenas. We complement our findings with further examples of other CALIOP measurements in coastal environments including observations at Hawaii (Pacific), Tasmania (Pacific), Ireland (Atlantic), and Cuba (Atlantic, Sect. 3.3). In Sect. 3.4 simplified radiative-transfer calculations were performed for clean marine and polluted conditions in the planetary boundary layer. Finally, a summary of the findings is given in Sect. 4.

2 Experiment

2.1 Field site

The mobile facility OCEANET-Atmosphere of the Leibniz Institute for Tropospheric Research (TROPOS) performs aerosol and cloud observation with a Raman/polarization lidar on a regular basis during the meridional transatlantic cruises of the research vessel Polarstern between northern and southern midlatitudes (Kanitz et al., 2013). While Polarstern moved on to Antarctica during the southern-hemispheric Summer of 2009/2010, the time period between the tracks (26 November 2009–17 April 2010) was used to perform aerosol observations with lidar at Punta Arenas, Chile (53° S, 71° W). In the framework of the Aerosol Lidar measurements at Punta Arenas in a Chilean germAn cooperation (ALPACA) campaign from 4 December 2009 to 4 April 2010, the TROPOS lidar Polly^{XT} was deployed at the Universidad de Magallanes. Punta Arenas is located at the Strait of the Magallanes (Fig. 1a). In the west direction rugged spurs of the Anden Mountains and in the east direction grassy fields dominate the orography. Constant westerly to north westerly air flows prevail throughout the year

**CALIPSO surface
type effect on aerosol
type**

T. Kanitz et al.

Title Page

Abstract

Introduction

Conclusions

References

Tables

Figures

◀

▶

◀

▶

Back

Close

Full Screen / Esc

Printer-friendly Version

Interactive Discussion



with a mean surface speed of 4.6 m s^{-1} which is caused by the Antarctic low-pressure belt (Schneider et al., 2003). Figure 1b shows a map of the Southern Hemisphere. Geopotential height at 500 hPa is denoted by the color code for 1 January 2010 in Fig. 1b. Dark colors indicate the low-pressure systems around the Antarctic. Air masses are advected along the isohypses (black contour lines in Fig. 1b). As it is clearly shown in Fig. 1b, the air masses that are advected to Punta Arenas pass over no other continental areas and are usually of pure marine origin.

Close to Punta Arenas, AERONET observations have been performed 200 km north-east in Rio Gallegos, Argentina at the Atlantic coast since November 2005 (Fig. 1a). The meteorological conditions are similar at Rio Gallegos and at Punta Arenas.

2.2 Polly^{XT}

Polly^{XT} measures backscattered light at wavelengths of 355, 532, and 1064 nm and Raman scattered light at 387 and 607 nm in order to determine profiles of the particle backscatter coefficient at three wavelengths and the extinction coefficient at 355 and 532 nm. A polarization-sensitive channel detects light at 355 nm and allows the determination of the particle linear depolarization ratio (Freudenthaler et al., 2009). Polly^{XT} data is acquired at a vertical and temporal resolution of 30 m and 30 s, respectively. The system was operated 24/7 and controlled remotely by TROPOS via internet access during the whole campaign.

In the analysis of the observations, we had to deal with two deficiencies. In the near range ($< 400 \text{ m}$), the signal of the bistatic system is corrupted by an incomplete overlap of the laser beam with the receiver field of view. As a consequence values of the particle backscatter coefficient were set constant below 400-m height in dependence of the planetary boundary layer height. In doing so, we assume well-mixed conditions in the lower part of the planetary boundary layer, which was found to be sufficient under marine conditions (Kanitz et al., 2013).

CALIPSO surface type effect on aerosol type

T. Kanitz et al.

Title Page

Abstract

Introduction

Conclusions

References

Tables

Figures



Back

Close

Full Screen / Esc

Printer-friendly Version

Interactive Discussion



In addition, the 355-nm channels did not work properly during ALPACA. The backscatter coefficient at 532 nm was determined from the ratio of the inelastic and elastic backscatter signal (Ansmann and Müller, 2005). But because of the rather low aerosol content, the inelastic signals could not be used for direct extinction-coefficient profiling. The particle extinction coefficient had to be estimated from the 532-nm backscatter coefficient by means of appropriate S_p values in combination with AERONET Sun photometer observations of the total atmospheric AOT. Accounting for the spatial separation of the two measurement sites, HYSPLIT-trajectory analyses (Draxler and Rolph, 2003) and an aerosol transport model (namely the Navy Aerosol Analysis and Prediction System, NAAPS) were incorporated to align lidar and Sun photometer observations. A simplified statistical approach will be discussed in Sect. 3.2.

2.3 AERONET Sun photometer

An AERONET (Holben et al., 1998) station is located at Rio Gallegos, Argentina (CEILAP-RG). The AERONET Sun photometer measures AOT (column-integrated extinction coefficient) from 340 to 1020 nm at 7 channels. In our analysis we used the level 2.0 data. The uncertainty in the AOT values is 0.01–0.02 (Holben et al., 2001).

2.4 CALIOP

CALIOP is an elastic-backscatter lidar that orbits the Earth at a height of 705 km with a velocity of 7000 m s^{-1} . Based on the laser footprint the lidar covers 0.2 % of the Earth's surface during one repeat cycle (Kahn et al., 2008). It passes over the same location each 16th day. CALIOP measures backscattering at 532 and 1064 nm and depolarization at 532 nm. The system and data analysis is explained by Winker et al. (2009). Within the present study, we focus on the level 2 version 3 data obtained for the wavelength of 532 nm. The level 2 data provide profiles of the particle backscatter and extinction coefficient, as well as information about the determined feature type (e.g.,

clouds or aerosols) and aerosol subtype (e.g., dust, smoke). Furthermore, quality flags are provided for each data point.

We used the Cloud-Aerosol Discrimination (CAD) score (Liu et al., 2009), the feature classification flags (Omar et al., 2009), and the extinction flag (Young and Vaughan, 2009) for the data quality assurance. We set conservative thresholds of CAD score ≤ 90 (observed layer contains particles with very high probability, optically thin marine boundary layer clouds are avoided), feature subtyping flag = 1 (confident aerosol subtyping), and extinction flag = 0 (no changes of S_p within the Hybrid Extinction Retrieval Algorithm are allowed). The obtained surface type is given by the International Geosphere-Biosphere Programme (IGBP, 1990) map and the position information of CALIOP itself.

2.5 Library for radiative transfer (libRadtran)

Radiative-transfer calculations were performed with the UVSPEC program (Kylling, 1992) of the libRadtran library version 1.6-beta (Mayer and Kylling, 2005). Broadband solar downward and upward irradiances were calculated in the wavelength range from 245 to 4500 nm to estimate the direct solar aerosol radiative effect (SARE) at the surface and the top of atmosphere (TOA). The libRadtran library includes the spectral integration by the correlated-k approximation (Kato et al., 1999) and the discrete ordinate solver DISORT version 2.0 (Stamnes et al., 1988). DISORT was applied with 16 streams. Solar zenith angles were determined as a function of latitudinal belt (10° steps from 50° N to 50° S), season (15 January, April, July, and October), and in steps of 15 min per day (Blanco-Muriel et al., 2001). Particle-free and cloud-free atmospheric conditions were described with US standard atmosphere (Anderson et al., 1986) as implemented in libRadtran for trace gases, pressure, temperature, and relative humidity. Aerosol single-scattering albedo and asymmetry parameter were taken from Dubovik et al. (2002).

CALIPSO surface type effect on aerosol type

T. Kanitz et al.

Title Page

Abstract

Introduction

Conclusions

References

Tables

Figures



Back

Close

Full Screen / Esc

Printer-friendly Version

Interactive Discussion



3 Results

We begin with a case study of a homogeneous aerosol layer observed with Polly^{XT} and CALIOP in the area of Punta Arenas. The found patterns in the CALIOP aerosol subtype mask gave evidence of a surface-dependent aerosol characterization within the CALIOP data algorithm. Afterwards, the general aerosol conditions in the area of Punta Arenas are analyzed based on the ground-based Polly^{XT} observations and AERONET long-term monitoring. The results are contrasted to the CALIPSO long-term measurements to check the impact of the surface-related effect on the CALIPSO-derived aerosol statistics. We finish the analysis with further CALIOP observations in rather different coastal environments to corroborate our case study analyses at Punta Arenas. A simplified study on the influence of aerosol mistyping on radiative-transfer calculations is presented at the end.

3.1 A case study of artificial patterns in a homogeneous aerosol layer

Figure 2 shows the observation of Polly^{XT} for the period from 02:00 to 06:00 UTC on 13 January 2010. Patterns of clouds in 2, 7, and 10 km height as well as an aerosol layer reaching to 1.5 km height can be seen. Within this measurement period CALIPSO passed over Punta Arenas at a distance of about 150 km indicated by a thin red line and a red star in Fig. 3a. In addition, grey and bright areas show water surfaces and land surfaces, respectively, as determined within IGBP. In the surrounding of Punta Arenas, grey areas indicate the rugged coastline and the large water surfaces of the Strait of the Magellanes (see also Fig. 1a). The vertical distribution and structure of the cloud and aerosol layers in the selected data subset of CALIOP (thick red line in Fig. 3a) is in excellent agreement with the patterns of the Polly^{XT} observation (cf. Figs. 2 and 3b).

Figure 3c presents the feature type mask of the data subset for the period indicated by the box with white frames in Fig. 3b. Green and dark blue coloring in Fig. 3c indicate the surface elevation and aerosol-free atmosphere, respectively. Data points for which no aerosol and cloud information could be retrieved due to strong attenuation

Title Page

Abstract

Introduction

Conclusions

References

Tables

Figures



Back

Close

Full Screen / Esc

Printer-friendly Version

Interactive Discussion



CALIPSO surface type effect on aerosol type

T. Kanitz et al.

Title Page

Abstract

Introduction

Conclusions

References

Tables

Figures

◀

▶

◀

▶

Back

Close

Full Screen / Esc

Printer-friendly Version

Interactive Discussion



of the laser beam are colored black. Data points of uncertain feature type are colored red. In the beginning of the measurement period aerosol (orange color) was identified up to 1.5 km below clouds (light blue) and even within the clouds. The subtype mask in Fig. 3d shows abrupt changes between mainly polluted continental aerosol (with smoke embedded) and marine aerosol from left to right, indicated by the change of red and blue. We added the surface type information in terms of a Google Earth map (Fig. 3e) and from the IGBP map (Fig. 3f). Yellow patterns indicate land surfaces and light blue patterns indicate water surfaces in Fig. 3f. The change in the determined aerosol type from polluted continental aerosol to marine aerosol is associated with the change in the surface type from land to ocean. The switch from red/black to blue columns can be observed in the course of the measurement on 13 January 2010 two times (Fig. 3d) although the height-time cross-section of the CALIOP-derived attenuated backscatter (Fig. 3b) indicates a homogeneous boundary-aerosol layer, similar to the higher temporal and vertical-resolved measurement of Polly^{XT} (Fig. 2).

Particle backscatter coefficients from CALIOP level 2 data for cloud-free signals were selected for the scene shown in Fig. 3d. Figure 4a presents profiles of the particle backscatter coefficient at 532 nm determined with Polly^{XT} (green line) and CALIOP (black line). The black curve differs only slightly from the green curve in magnitude. Figure 4b shows the mean profiles of the particle backscatter coefficient as derived with CALIOP measurements over water (blue) and over land (red) without clouds. The profiles indicate similar backscatter conditions over land and water. In contrast to the two particle backscatter profiles, the respective mean extinction coefficients deviate strongly. Over the water surface the aerosol layer is identified as marine aerosol and the backscatter coefficients are multiplied by S_p of 20 sr. Instead, over land the aerosol layer was interpreted partly as polluted continental aerosol, partly as smoke, and sometimes as clean continental aerosol. Thus, the extinction coefficients are computed from the backscatter coefficients by using $S_p = 35$ sr (clean continental) and mostly $S_p = 70$ sr (polluted continental and smoke). As a result, the extinction coefficients

determined in a more or less homogeneous aerosol layer over land are about 3.5 times higher than over water surface (Fig. 4c).

3.2 A possible overestimation of strong absorbing continental aerosol at Punta Arenas

5 The surface-type dependence of the aerosol typing within the CALIOP data algorithm may affect general long-term aerosol studies with CALIOP at coastal regions. In the framework of ALPACA the ground-based lidar observations of Polly^{XT} at Punta Arenas and the AERONET Sun photometer observations at Rio Gallegos were used to determine the AOT frequency distribution for the period from 4 December 2009 to
10 4 April 2010 during cloud-free conditions.

Within this approach, the lidar profiles of the particle backscatter coefficient were vertically integrated and multiplied with S_p of 20, 35, and 70 sr, representing marine, clean continental, and polluted continental aerosol conditions, respectively. Figure 5a shows the AOT frequency distribution as derived with Sun photometer at Rio
15 Gallegos. In > 95 % out of all cases the AOT is < 0.05. Assuming almost similar aerosol conditions at Punta Arenas and Rio Gallegos, the lidar-derived AOT distribution determined with a S_p of 20 sr shows the best agreement with the AERONET-derived AOT distribution. The assumption of the presence of polluted continental aerosol or smoke, so that S_p of 70 sr is appropriate, leads to an unrealistic AOT statistics for this
20 rather clean environment (Fig. 5c). The very low annual AOT of ≈ 0.02 (2009, 2010) from AERONET observations indicates clean marine conditions as well (Smirnov et al., 2009; Wilson and Forgan, 2002).

In the next step, CALIOP level 2 version 3 data were analyzed for the ALPACA campaign. For CALIPSO overflights within a distance of 200 km to Punta Arenas (Anderson et al., 2003) HYSPLIT-trajectory analyses enabled us to select the part of the CALIPSO
25 track that relates best to the 24/7 measurements of Polly^{XT} at Punta Arenas (Tesche et al., 2013). A cross section was defined to consist of 40–50 profiles to account for frequently occurring clouds (Kanitz et al., 2011) that totally attenuate the laser beam of

CALIPSO surface type effect on aerosol type

T. Kanitz et al.

Title Page

Abstract

Introduction

Conclusions

References

Tables

Figures



Back

Close

Full Screen / Esc

Printer-friendly Version

Interactive Discussion



(height < 1 km), marine aerosol is determined in 48 % out of all cases over water surface and in 11 % out of all cases over land surfaces. Instead, strong absorbing aerosol was found more often over land surface (71 %) than over water surface (38 %).

3.3 CALIOP aerosol typing at other coastal regions

5 Further examples of CALIOP measurements in coastal regions and aerosol background conditions are presented in Fig. 8. The abscissa in Fig. 8a–h shows the coordinates of the CALIPSO flight track in terms of latitude (upper row, south < 0) and longitude (lower row, west < 0). On 24 December 2009 (nighttime) CALIPSO passed over Mauna Loa, Hawaii (Fig. 8a). According to the CALIOP level 2 data, marine aerosol was
10 observed around Mauna Loa indicated by blue color in Fig. 8e. As soon as CALIOP measured over land the boundary-layer aerosol was classified as smoke and polluted continental aerosol. As explained before, the change in the aerosol type is associated with the use of a significantly increased S_p value. Figure 8i shows the averaged profiles of the 532 nm backscatter and extinction coefficients by dashed and solid lines, respectively,
15 for the aerosol conditions in Fig. 8e. Blue and red lines indicate profiles acquired over water and land surface, respectively. The error bars are the root of the summed squares of the error provided in the CALIOP level 2 data for each profile. Although the backscatter coefficients show almost equal values from 1–2 km height, the extinction coefficients show a difference of a factor of 3–4. The same pattern can be seen in terms
20 of an overflight of CALIPSO over Tasmania on 16 November 2011 (nighttime, Fig. 8b, f, and j). Two other measurement examples were taken from the CALIPSO data set in the area of the Atlantic Ocean. On 4 September 2009 (nighttime, Fig. 8k) and 1 November 2011 (daytime, Fig. 8l) CALIOP-retrieved profiles of the 532-nm backscatter coefficient over water and land surface are in good agreement and indicate homogeneous aerosol layers along the selected overflights of CALIPSO over Ireland and Cuba.
25 Nevertheless, strong differences between the respective extinction values (over water vs. over land) occurred due to the used subtyping in the CALIOP data analysis.

CALIPSO surface type effect on aerosol type

T. Kanitz et al.

Title Page

Abstract

Introduction

Conclusions

References

Tables

Figures



Back

Close

Full Screen / Esc

Printer-friendly Version

Interactive Discussion



3.4 Radiative effect of marine and polluted aerosol

A simple assessment study was performed to estimate the solar aerosol radiative effect (SARE) of the planetary boundary layer for pure marine and polluted aerosol conditions. The difference in SARE (pure marine vs. polluted) indicates the magnitude of the bias in the aerosol radiative effect caused by the surface effect in the CALIOP data analysis at coastal sites. For both scenarios the boundary layer top was set to 0.8 km height and well-mixed conditions (constant aerosol extinction profile) were assumed in the boundary layer. The AOT was set to 0.05 in the scenario of marine conditions on the basis of global Sun photometer observations (Smirnov et al., 2009). In accordance to the CALIOP data algorithm the AOT was defined 3.5 times higher to 0.175 in the scenario for polluted conditions. The information on single scattering albedo, and asymmetry parameter were taken from AERONET for marine aerosol and polluted continental aerosol, the measurement results from Lanai and the Maldives respectively (cf. Table 1 in Dubovik et al., 2002). Table 1 gives an overview for both scenarios. The surface albedo was set to 0.2 to represent surface conditions between deserts (0.2–0.45) and different vegetation (0.05–0.25).

Figure 9 (top and bottom panel) shows the SARE of the boundary layer at the top of atmosphere (TOA) and the surface for different latitudes and seasons, represented by the 15 January, April, July, and October. At the TOA the SARE in both scenarios is almost similar and ranges from -1 W m^{-2} to -4 W m^{-2} with season and latitude (Fig. 9a and c). The difference of the SARE at the TOA, i.e., the impact of the different aerosol conditions on the SARE is less than 2 W m^{-2} as indicated in Fig. 9e. Consequently, the higher AOT and the higher absorption (lower single scattering albedo) in the scenario for polluted aerosol conditions in the boundary layer do not significantly alter the planetary albedo for incident radiation in comparison to pure marine conditions. In contrast, the SARE at the surface shows large deviations for the simulations of both scenarios (Fig. 9b and d). In the scenario for polluted aerosol conditions, the higher AOT and the efficient absorption of incident radiation increases the SARE from

CALIPSO surface type effect on aerosol type

T. Kanitz et al.

Title Page

Abstract

Introduction

Conclusions

References

Tables

Figures



Back

Close

Full Screen / Esc

Printer-friendly Version

Interactive Discussion



maximum -4 W m^{-2} (marine conditions) to maximum -17 W m^{-2} (polluted conditions). The difference in the SARE ranges from 5 to 13 W m^{-2} (Fig. 9f).

Additional simulations were performed for surface albedos of 0.05, 0.2, and 0.4 at 0° latitude and longitude on 15 April. Table 2 indicates the sensitivity of the surface albedo on the SARE at TOA. For surface albedos of 0.05 and 0.4 SARE at TOA changes by 3.5 and 5 W m^{-2} when the aerosol type changes from marine to polluted (Table 2). In the case of a surface albedo of 0.4 the SARE changes from a cooling effect (negative SARE) of -0.2 W m^{-2} under marine conditions to a warming effect (positive SARE) of 4.8 W m^{-2} for a boundary layer with polluted aerosol. At the surface, SARE decreases with increasing surface albedo for both aerosol conditions. The difference between the SARE decreases from -12.6 W m^{-2} and -7.3 W m^{-2} for surface albedos from 0.05 to 0.4, respectively.

The obtained simulation results shown in Fig. 9 represent worst-case scenarios based on the AOT of 0.05 for marine conditions (Smirnov et al., 2009). In the area of Punta Arenas, the mean AOT is below 0.05. Radiative-transfer calculations were repeated for both scenarios based on an AOT value of 0.02 for marine conditions at 0° latitude and longitude in Spring, on 15 April respectively. The AOT was set to 0.07 for polluted aerosol conditions. Table 3 presents the SARE for different aerosol conditions and AOTs. In agreement to Fig. 9 the SARE at TOA is almost similar for both scenarios and AOT values as found in the area of Punta Arenas, if the simulations are performed for a surface albedo of 0.2 (cf. Table 2). At the surface SARE decreases with the decreased AOT (0.05–0.02) from -2.5 to -1.0 W m^{-2} for marine conditions and from -12.7 to -5.5 W m^{-2} for a boundary layer with polluted aerosol and AOTs of 0.175 to 0.07. Finally, the difference between both scenarios is 4.5 W m^{-2} for the approach with lower AOTs. In summary, a bias in studies of surface SARE can not be excluded when aerosol conditions are based on CALIOP extinction profiles at coastal sites, as a consequence of the surface-effect in the CALIOP data analysis.

CALIPSO surface type effect on aerosol type

T. Kanitz et al.

Title Page

Abstract

Introduction

Conclusions

References

Tables

Figures

◀

▶

◀

▶

Back

Close

Full Screen / Esc

Printer-friendly Version

Interactive Discussion



4 Conclusions

By analyzing coincident measurements of the CALIOP lidar, AERONET Sun photometer, and Polly^{XT} lidar at the rugged coastline of southern Latin America, clean atmospheric background conditions (AOT of ≈ 0.02) were investigated which are representative for the latitudinal belt from 50° S to 60° S. In this area, the Antarctic low-pressure belt advects constantly air masses from the Southern Oceans, and continental aerosol sources are almost absent. Consequently, AERONET, and Polly^{XT} observations revealed clean marine aerosol conditions mixed with local clean continental aerosol in southern Latin America. However, the automated CALIOP data analysis classified in about 70 % out of all cases the detected aerosol as polluted dust, polluted continental aerosol, or smoke. Within a case study, this discrepancy was found to be the result of the surface-dependent CALIOP data analysis, including the prohibition of marine aerosol over land with crucial effects on the determination of vertical profiles of extinction and an increase of the AOT by a factor of up to 3.5. Worldwide observations of CALIOP at other coastal regions of Mauna Loa (Pacific), Tasmania (Pacific), Ireland (Atlantic), and Cuba (Atlantic) show the same patterns in the surface-dependent aerosol subtyping of CALIOP and a probable overestimation of the AOT in coastal areas over land. In simplified radiative-transfer simulations, two scenarios of boundary aerosol conditions were considered, marine aerosol and polluted continental aerosol, respectively. At the surface, a difference of 5 W m^{-2} to 13 W m^{-2} in the daily averaged direct solar aerosol radiative effect were found independent of the latitude and season. In ongoing investigations global aerosol transport models might be used to estimate the global impact of a possible aerosol misidentification in coastal areas. At the same time it might be appropriate to account for the coastline effect in the CALIOP data algorithm by using the CALIPSO satellite GPS information and by introducing an additional aerosol type, e.g., mixed marine aerosol for coastal areas.

AMTD

7, 1333–1365, 2014

CALIPSO surface type effect on aerosol type

T. Kanitz et al.

Title Page

Abstract

Introduction

Conclusions

References

Tables

Figures



Back

Close

Full Screen / Esc

Printer-friendly Version

Interactive Discussion



Acknowledgements. We thank the NASA Langley Research Center and the CALIPSO science team for the permanent effort and improvement of the CALIPSO data. Supplement from AERONET Sun photometer measurements, HYSPLIT trajectories, radiative-transfer calculations with libRadtran, and NASA CERES/SARB surface mapping within the International Geosphere-Biosphere Programme were a cornerstone of our data analysis.

References

- Althausen, D., Engelmann, R., Baars, H., Heese, B., Ansmann, A., Müller, D., and Komppula, M.: Portable Raman lidar Polly^{XT} for automated profiling of aerosol backscatter, extinction, and depolarization, *J. Atmos. Ocean. Tech.*, 26, 2366–2378, doi:10.1175/2009JTECHA1304.1, 2009. 1336
- Anderson, G. P., Clough, S. A., Kneizys, F. X., Chetwynd, J. H., and Shettle, E. P.: AFGL atmospheric constituent profiles (0.120 km), available at: <http://oai.dtic.mil/oai/oai?verb=getRecord&metadataPrefix=html&identifier=ADA175173> (last access: 7 February 2014), 1986. 1340
- Anderson, T. L., Charlson, R. J., Winker, D. M., Ogren, J. A., and Holmén, K.: Mesoscale variations of tropospheric aerosols, *J. Atmos. Sci.*, 60, 119–136, doi:10.1175/1520-0469(2003)060<0119:MVOTA>2.0.CO;2, 2003. 1343
- Ansmann, A. and Müller, D.: Lidar and atmospheric aerosol particles, in: *Lidar: Range-resolved optical remote sensing of the atmosphere*, edited by: Weitkamp, C., Springer, 105–138, 2005. 1339
- Bates, T. S., Huebert, B. J., Gras, J. L., Griffiths, F. B., and Durkee, P. A.: International Global Atmospheric Chemistry (IGAC) project's first Aerosol Characterization Experiment (ACE 1): overview, *J. Geophys. Res.*, 103, 16297–16318, doi:10.1029/97JD03741, 1998. 1336
- Blanco-Muriel, M., Alarcn-Padilla, D. C., Lpez-Moratalla, T., and Lara-Coira, M.: Computing the solar vector, *Sol. Energy*, 70, 431–441, doi:10.1016/S0038-092X(00)00156-0, 2001. 1340
- Bridhikitti, A.: Atmospheric aerosol layers over Bangkok Metropolitan Region from CALIPSO observations, *Atmos. Res.*, 127, 1–7, doi:10.1016/j.atmosres.2013.02.008, 2013. 1336
- Burton, S. P., Ferrare, R. A., Vaughan, M. A., Omar, A. H., Rogers, R. R., Hostetler, C. A., and Hair, J. W.: Aerosol classification from airborne HSRL and comparisons with the CALIPSO

CALIPSO surface type effect on aerosol type

T. Kanitz et al.

Title Page

Abstract

Introduction

Conclusions

References

Tables

Figures

◀

▶

◀

▶

Back

Close

Full Screen / Esc

Printer-friendly Version

Interactive Discussion



CALIPSO surface type effect on aerosol type

T. Kanitz et al.

Title Page

Abstract

Introduction

Conclusions

References

Tables

Figures

◀

▶

◀

▶

Back

Close

Full Screen / Esc

Printer-friendly Version

Interactive Discussion

vertical feature mask, *Atmos. Meas. Tech.*, 6, 1397–1412, doi:10.5194/amt-6-1397-2013, 2013. 1335

Draxler, R. R. and Rolph, G. D.: HYSPLIT (HYbrid Single-Particle Lagrangian Integrated Trajectory) model access via NOAA ARL READY website, available at: <http://www.arl.noaa.gov/ready/hysplit4.html> (last access: 7 February 2014), NOAA Air Resources Laboratory, Silver Spring, 2003. 1339

Dubovik, O., Holben, B., Eck, T. F., Smirnov, A., Kaufman, Y. J., King, M. D., Tarré, D., and Slutsker, I.: Variability of absorption and optical properties of key aerosol types observed in worldwide locations, *J. Atmos. Sci.*, 59, 590–608, doi:10.1175/1520-0469(2002)059<0590:VOAAOP>2.0.CO;2, 2002. 1340, 1346, 1354

Freudenthaler, V., Esselborn, M., Wiegner, M., Heese, B., Tesche, M., Ansmann, A., Müller, D., Althausen, D., Wirth, M., Fix, A., Ehret, G., Knippertz, P., Toledano, C., Gasteiger, J., Garhammer, M., and Seefeldner, M.: Depolarization ratio profiling at several wavelengths in pure Saharan dust during SAMUM 2006, *Tellus B*, 61, 165–179, doi:10.1111/j.1600-0889.2008.00396.x, 2009. 1338

Holben, B. N., Eck, T. F., Slutsker, I., Tanre, D., Buis, J. P., Setzer, A., Vermote, E., Reagan, J. A., Kaufman, Y. J., Nakajima, T., Lavenu, F., Jankowiak, I., and Smirnov, A.: AERONET – a federated instrument network and data archive for aerosol characterization, *Remote Sens. Environ.*, 66, 1–16, doi:10.1016/S0034-4257(98)00031-5, 1998. 1339

Holben, B. N., Tarré, D., Smirnov, A., Eck, T. F., Slutsker, I., Abuhassan, N., Newcomb, W. W., Schafer, J. S., Chatenet, B., Lavenu, F., Kaufman, Y. J., Vande Castle, J., Setzer, A., Markham, B., Clark, D., Frouin, R., Halthore, R., Karneli, A., O'Neill, N. T., Pietras, C., Pinker, R. T., Voss, K., and Zibordi, G.: An emerging ground-based aerosol climatology: aerosol optical depth from AERONET, *J. Geophys. Res.*, 106, 12067–12097, doi:10.1029/2001JD900014, 2001. 1339

Huang, J., Fu, Q., Su, J., Tang, Q., Minnis, P., Hu, Y., Yi, Y., and Zhao, Q.: Taklimakan dust aerosol radiative heating derived from CALIPSO observations using the Fu-Liou radiation model with CERES constraints, *Atmos. Chem. Phys.*, 9, 4011–4021, doi:10.5194/acp-9-4011-2009, 2009. 1334

IGBP: The International Geosphere-Biosphere Programme: a study of global change-the initial core project, IGBP Global Change Report no. 12, International Geosphere-Biosphere Programme, Stockholm, Sweden, available at: http://www-surf.larc.nasa.gov/surf/pages/sce_type.html (last access: 7 February 2014), 1990. 1340, 1359, 1362

CALIPSO surface type effect on aerosol type

T. Kanitz et al.

Title Page

Abstract

Introduction

Conclusions

References

Tables

Figures

◀

▶

◀

▶

Back

Close

Full Screen / Esc

Printer-friendly Version

Interactive Discussion



- Kahn, R. A., Chen, Y., Nelson, D. L., Leung, F. Y., Li, Q., Diner, D. J., and Logan, J. A.: Wildfire smoke injection heights: two perspectives from space, *Geophys. Res. Lett.*, 35, L04809, doi:10.1029/2007GL032165, 2008. 1339
- 5 Kanitz, T., Seifert, P., Ansmann, A., Engelmann, R., Althausen, D., Casiccia, C., and Rohwer, E. G.: Contrasting the impact of aerosols at northern and southern midlatitudes on heterogeneous ice formation, *Geophys. Res. Lett.*, 38, L17802, doi:10.1029/2011GL048532, 2011. 1343
- 10 Kanitz, T., Ansmann, A., Engelmann, R., and Althausen, D.: North-south cross sections of aerosol layering over the Atlantic Ocean from multiwavelength Raman/polarization lidar during Polarstern cruises., *J. Geophys. Res.*, 118, 2643–2655, doi:10.1002/jgrd.50273, 2013. 1337, 1338
- Kato, S., Ackerman, T. P., Mather, J. H., and Clothiaux, E. E.: The k-distribution method and correlated-k approximation for a shortwave radiative transfer model, *J. Quant. Spectrosc. Ra.*, 62, 109–121, doi:10.1016/S0022-4073(98)00075-2, 1999. 1340
- 15 Kylling, A.: Radiation transport in cloudy and aerosol loaded atmospheres, Ph. D. thesis, Alaska University, Fairbanks, 1992. 1340
- Liu, D., Wang, Z., Liu, Z., Winker, D., and Trepte, C.: A height resolved global view of dust aerosols from the first year CALIPSO lidar measurements, *J. Geophys. Res.*, 113, D16214, doi:10.1029/2007JD009776, 2008. 1334
- 20 Liu, Z., Vaughan, M., Winker, D., Kittaka, C., Getzewich, B., Kuehn, R., Omar, A., Powell, K., Trepte, C., and Hostetler, C.: The CALIPSO lidar cloud and aerosol discrimination: Version 2 algorithm and initial assessment of performance, *J. Atmos. Ocean. Tech.*, 26, 1198–1213, doi:10.1175/2009JTECHA1229.1, 2009. 1335, 1340
- Lopes, F. J. S., Landulfo, E., and Vaughan, M. A.: Evaluating CALIPSO's 532 nm lidar ratio selection algorithm using AERONET sun photometers in Brazil, *Atmos. Meas. Tech.*, 6, 3281–3299, doi:10.5194/amt-6-3281-2013, 2013. 1335
- 25 Mamouri, R. E., Amiridis, V., Papayannis, A., Giannakaki, E., Tsaknakis, G., and Balis, D. S.: Validation of CALIPSO space-borne-derived attenuated backscatter coefficient profiles using a ground-based lidar in Athens, Greece, *Atmos. Meas. Tech.*, 2, 513–522, doi:10.5194/amt-2-513-2009, 2009. 1335
- 30 Mayer, B. and Kylling, A.: Technical note: The libRadtran software package for radiative transfer calculations – description and examples of use, *Atmos. Chem. Phys.*, 5, 1855–1877, doi:10.5194/acp-5-1855-2005, 2005. 1340

CALIPSO surface type effect on aerosol type

T. Kanitz et al.

Title Page

Abstract

Introduction

Conclusions

References

Tables

Figures

◀

▶

◀

▶

Back

Close

Full Screen / Esc

Printer-friendly Version

Interactive Discussion



- Miller, S. T. K., Keim, B. D., Talbot, R. W., and Mao, H.: Sea breeze: structure, forecasting, and impacts, *Rev. Geophys.*, 41, 1011, doi:10.1029/2003RG000124, 2003. 1336
- Omar, A. H., Winker, D. M., Kittaka, C., Vaughan, M. A., Liu, Z., Hu, Y., Trepte, C. R., Rogers, R. R., Ferrare, R. A., Lee, K. P., Kuehn, R. E., and Hostetler, C. A.: The CALIPSO automated aerosol classification and lidar ratio selection algorithm, *J. Atmos. Ocean. Tech.*, 26, 1994–2014, doi:10.1175/2009JTECHA1231.1, 2009. 1335, 1336, 1340
- Omar, A. H., Winker, D. M., Tackett, J. L., Giles, D. M., Kar, J., Liu, Z., Vaughan, M. A., Powell, K. A., and Trepte, C. R.: CALIOP and AERONET aerosol optical depth comparisons: one size fits none, *J. Geophys. Res.*, 118, 4748–4766, doi:10.1002/jgrd.50330, 2013. 1336
- Oo, M. and Holz, R.: Improving the CALIOP aerosol optical depth using combined MODIS-CALIOP observations and CALIOP integrated attenuated total color ratio, *J. Geophys. Res.*, 116, D14201, doi:10.1029/2010JD014894, 2011. 1336
- Rogers, R. R., Hostetler, C. A., Hair, J. W., Ferrare, R. A., Liu, Z., Obland, M. D., Harper, D. B., Cook, A. L., Powell, K. A., Vaughan, M. A., and Winker, D. M.: Assessment of the CALIPSO Lidar 532 nm attenuated backscatter calibration using the NASA LaRC airborne High Spectral Resolution Lidar, *Atmos. Chem. Phys.*, 11, 1295–1311, doi:10.5194/acp-11-1295-2011, 2011. 1335
- Pappalardo, G., Wandinger, U., Mona, L., et al.: EARLINET correlative measurements for CALIPSO: first intercomparison results, *J. Geophys. Res.*, 115, D00H19, doi:10.1029/2009JD012147, 2010. 1335
- Schneider, C., Glaser, M., Kilian, R., Santana, A., Butorovic, N., and Casassa, G.: Weather observations across the southern Andes at 53° S, *Phys. Geogr.*, 24, 97–119, 2003. 1338
- Schuster, G. L., Vaughan, M., MacDonnell, D., Su, W., Winker, D., Dubovik, O., Lapyonok, T., and Trepte, C.: Comparison of CALIPSO aerosol optical depth retrievals to AERONET measurements, and a climatology for the lidar ratio of dust, *Atmos. Chem. Phys.*, 12, 7431–7452, doi:10.5194/acp-12-7431-2012, 2012. 1335, 1336
- Smirnov, A., Holben, B. N., Slutsker, I., et al.: Maritime Aerosol Network as a component of Aerosol Robotic Network, *J. Geophys. Res.*, 114, D06204, doi:10.1029/2008JD011257, 2009. 1343, 1346, 1347, 1354
- Stamnes, K., Tsay, S.-C., Jayaweera, K., and Wiscombe, W.: Numerically stable algorithm for discrete-ordinate-method radiative transfer in multiple scattering and emitting layered media, *Atmos. Opt.*, 27, 2502–2509, doi:10.1364/AO.27.002502, 1988. 1340

CALIPSO surface type effect on aerosol type

T. Kanitz et al.

Title Page

Abstract

Introduction

Conclusions

References

Tables

Figures

◀

▶

◀

▶

Back

Close

Full Screen / Esc

Printer-friendly Version

Interactive Discussion



Tesche, M., Wandinger, U., Ansmann, A., Althausen, D., Müller, D., and Omar, A. H.: Ground-based validation of CALIPSO observations of dust and smoke in the Cape Verde region, *J. Geophys. Res.*, 118, 2889–2902, doi:10.1002/jgrd.50248, 2013. 1335, 1343

5 Vaughan, M. A., Powell, K. A., Winker, D. M., Hostetler, C. A., Kuehn, R. E., Hunt, W. H., Getzewich, N. J., Young, S. A., Liu, Z., and McGill, M. J.: Fully automated detection of cloud and aerosol layers in the CALIPSO lidar measurements, *J. Atmos. Ocean. Tech.*, 26, 2034–2050, doi:10.1175/2009JTECHA1228.1, 2009. 1335

10 Wandinger, U., Tesche, M., Seifert, P., Ansmann, A., Müller, D., and Althausen, D.: Size matters: influence of multiple-scattering on CALIPSO light-extinction profiling in desert dust, *Geophys. Res. Lett.*, 37, L10801, doi:10.1029/2010GL042815, 2010. 1335

Wilson, S. R. and Forgan, B. W.: Aerosol optical depth at Cape Grim, Tasmania 1986–1999, *J. Geophys. Res.*, 107, 4068, doi:10.1029/2001JD000398, 2002. 1343

15 Winker, D. M., Vaughan, M. A., Omar, A., Hu, Y., Powell, K. A., Liu, Z., Hunt, W. H., and Young, S. A.: Overview of the CALIPSO mission and CALIOP data processing algorithms, *J. Atmos. Ocean. Tech.*, 26, 2310–2323, doi:10.1175/2009JTECHA1281.1, 2009. 1334, 1339

Winker, D. M., Tackett, J. L., Getzewich, B. J., Liu, Z., Vaughan, M. A., and Rogers, R. R.: The global 3-D distribution of tropospheric aerosols as characterized by CALIOP, *Atmos. Chem. Phys.*, 13, 3345–3361, doi:10.5194/acp-13-3345-2013, 2013. 1336

20 Young, S. A. and Vaughan, M. A.: The retrieval of profiles of particulate extinction from Cloud Aerosol Lidar Infrared Pathfinder Satellite Observations (CALIPSO) data: algorithm description, *J. Atmos. Ocean. Tech.*, 26, 1105–1119, doi:10.1175/2008JTECHA1221.1, 2009. 1335, 1340

25 Young, S. A., Vaughan, M. A., Kuehn, R. E., and Winker, D. M.: The retrieval of profiles of particulate extinction from Cloud Aerosol Lidar and Infrared Pathfinder Satellite Observations (CALIPSO) data: uncertainty and error sensitivity analyses, *J. Atmos. Ocean. Tech.*, 30, 395–428, doi:10.1175/JTECH-D-12-00046.1, 2013. 1335

CALIPSO surface type effect on aerosol type

T. Kanitz et al.

Table 1. Input parameter for simplified radiative-transfer calculations. Mean aerosol optical thickness (AOT) for marine conditions is taken from Smirnov et al. (2009), single scattering albedo (SSA) and asymmetry parameter (g) are taken from Dubovik et al. (2002).

Input for radiative-transfer calculations		
Scenario 1 (marine)	AOT	0.05
	Ångström	0.4
	SSA (440/670/870/1020)	0.98/0.97/0.97/0.97
	g (440/670/870/1020)	0.75/0.71/0.69/0.68
Scenario 2 (polluted)	AOT	0.175
	Ångström	0.8
	SSA (440/670/870/1020)	0.91/0.89/0.86/0.84
	g (440/670/870/1020)	0.74/0.67/0.64/0.63

[Title Page](#)
[Abstract](#)
[Introduction](#)
[Conclusions](#)
[References](#)
[Tables](#)
[Figures](#)
[Back](#)
[Close](#)
[Full Screen / Esc](#)
[Printer-friendly Version](#)
[Interactive Discussion](#)


CALIPSO surface type effect on aerosol type

T. Kanitz et al.

Table 2. Results of radiative-transfer calculations for different surface albedos. Pure marine and polluted aerosol conditions were simulated at 0° latitude and longitude in Spring (on 15 April). The settings for both scenarios are given in Table 1. TOA and SARE denote the top of atmosphere and the 24 h averaged solar aerosol radiative effect, respectively.

	Scenario	Aerosol	SARE (W m^{-2}) for albedos		
			0.05	0.20	0.40
Surface	1	marine	-3.5	-2.5	-1.4
	2	polluted	-16.1	-12.7	-8.7
TOA	1	marine	-2.5	-1.4	-0.2
	2	polluted	-6.0	-1.3	4.8

Title Page

Abstract

Introduction

Conclusions

References

Tables

Figures

◀

▶

◀

▶

Back

Close

Full Screen / Esc

Printer-friendly Version

Interactive Discussion



CALIPSO surface type effect on aerosol type

T. Kanitz et al.

Table 3. Results of radiative-transfer calculations for different aerosol optical thickness (AOT). Pure marine and polluted aerosol conditions were simulated for a surface albedo of 0.2 at 0° latitude and longitude in Spring (on 15 April). The settings for both scenarios are given in Table 1. TOA and SARE denote the top of atmosphere and the 24 h averaged solar aerosol radiative effect, respectively.

	Scenario	Aerosol	AOT	SARE (W m^{-2})
Surface	1	marine	0.020	-1.0
	2	polluted	0.070	-5.5
	1	marine	0.050	-2.5
	2	polluted	0.175	-12.7
TOA	1	marine	0.020	-0.6
	2	polluted	0.070	-0.6
	1	marine	0.050	-1.4
	2	polluted	0.175	-1.3

Title Page

Abstract

Introduction

Conclusions

References

Tables

Figures

◀

▶

◀

▶

Back

Close

Full Screen / Esc

Printer-friendly Version

Interactive Discussion



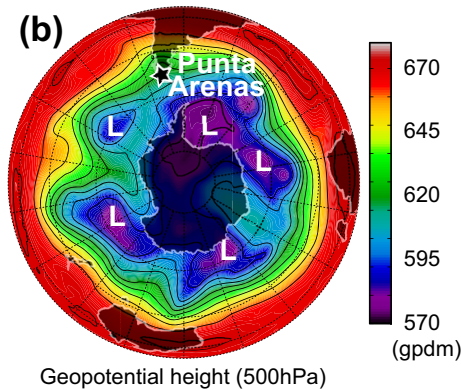
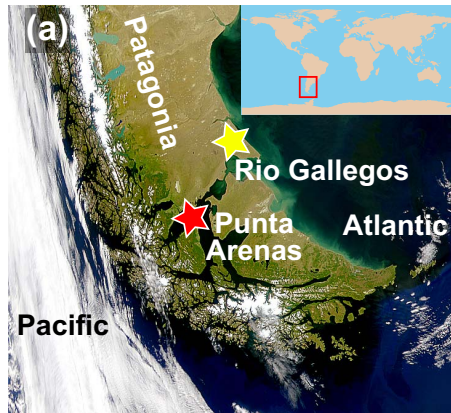


Fig. 1. (a) Map of the southern part of South America. **(b)** Map of the Southern Hemisphere. Geopotential height at 500 hPa is shown by the color code for 1 January 2010. L denotes low-pressure system. Punta Arenas is indicated by red **(a)** and black star **(b)**, Rio Gallegos by a yellow star **(a)**.

CALIPSO surface type effect on aerosol type

T. Kanitz et al.

Title Page

Abstract Introduction

Conclusions References

Tables Figures

⏪ ⏩

◀ ▶

Back Close

Full Screen / Esc

Printer-friendly Version

Interactive Discussion



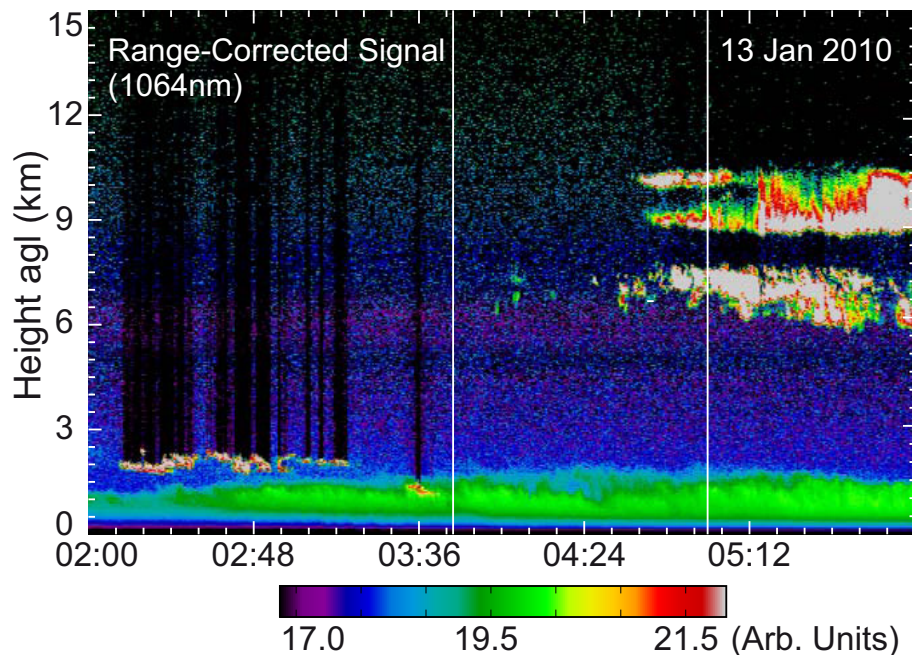


Fig. 2. Height-time cross-section of the range-corrected 1064-nm signal measured with Polly^{XT} at Punta Arenas on 13 January 2010, 02:00–06:00 UTC (night). White lines indicate the time period from 03:45–05:00 UTC as chosen for the comparison with the CALIOP measurement (see Fig. 3b).

CALIPSO surface type effect on aerosol type

T. Kanitz et al.

Title Page

Abstract Introduction

Conclusions References

Tables Figures

⏪ ⏩

◀ ▶

Back Close

Full Screen / Esc

Printer-friendly Version

Interactive Discussion



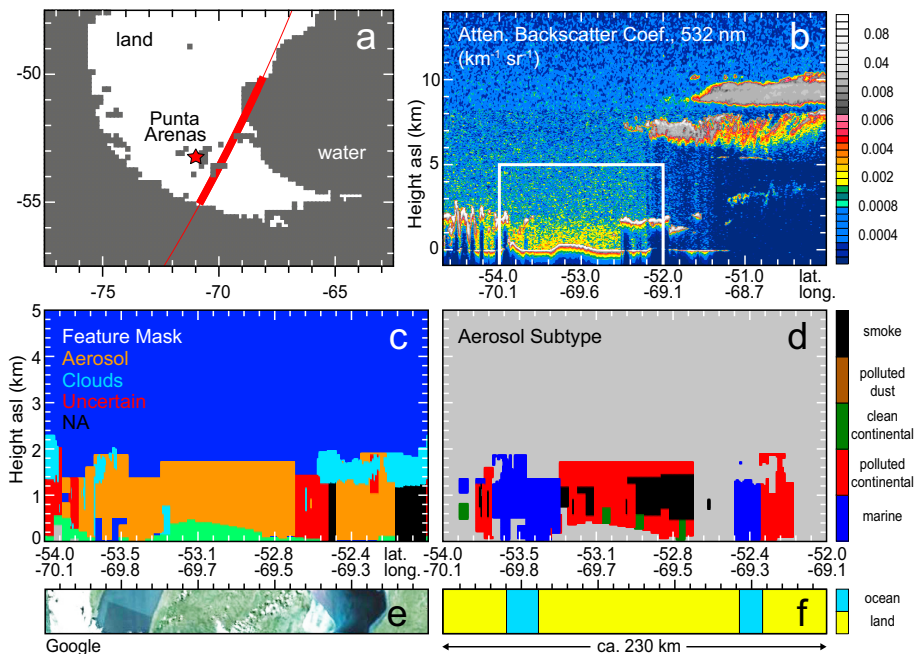


Fig. 3. (a) Map of the southernmost part of South America. The thin red line shows the CALIOP night overflight on 13 January 2010. The red star indicates Punta Arenas. The thick red-line segment indicates the selected time period of CALIOP in best agreement to the Polly^{XT} observation. (b) Height-time cross-section of the lidar attenuated backscatter at 532 nm of the CALIOP observation at 04:47 UTC on 13 January 2010 (for the thick red-line period in a). (c) Height-time cross-section of the vertical feature mask and (d) the aerosol subtype mask of the highlighted data subset in (b). Surface type information from the (e) Google Earth map and (f) the International Geosphere-Biosphere Programme (IGBP, 1990).

CALIPSO surface type effect on aerosol type

T. Kanitz et al.

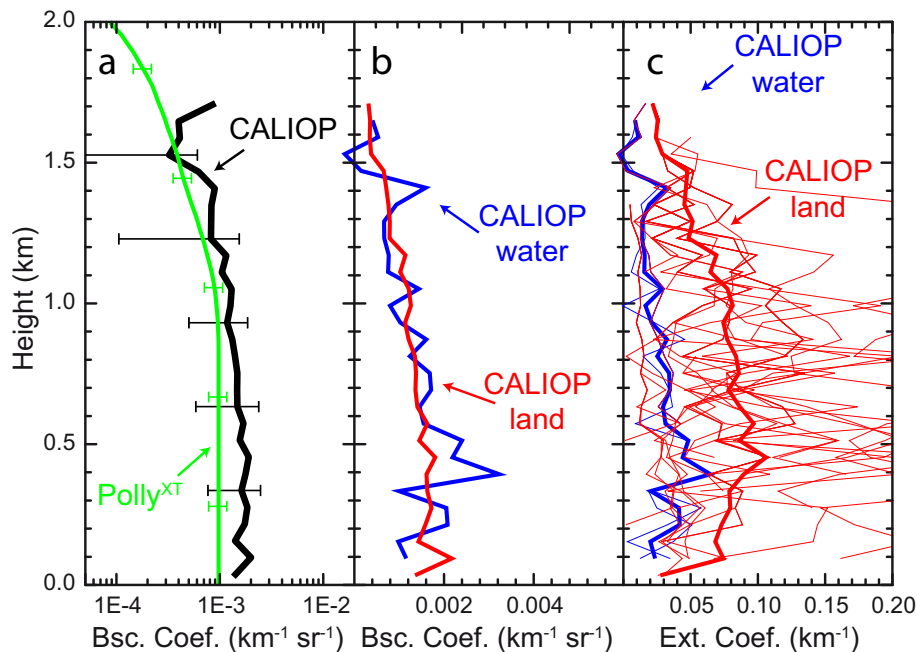


Fig. 4. (a) Mean vertical profiles of the particle backscatter coefficient at 532 nm as determined with Polly^{XT} (green) from 03:45 to 05:00 UTC and CALIOP at around 04:47 UTC on 13 January 2010. The CALIOP backscatter profiles are based on cloud-free signal profiles (black). (b) Averaged cloud-free profiles of the particle backscatter coefficient at 532 nm over land (red) and over water surface (blue) determined from CALIOP measurements. (c) Averaged cloud-free profiles of the extinction coefficient at 532 nm (thick lines) and individual profiles (thin lines).

Title Page

Abstract

Introduction

Conclusions

References

Tables

Figures

◀

▶

◀

▶

Back

Close

Full Screen / Esc

Printer-friendly Version

Interactive Discussion

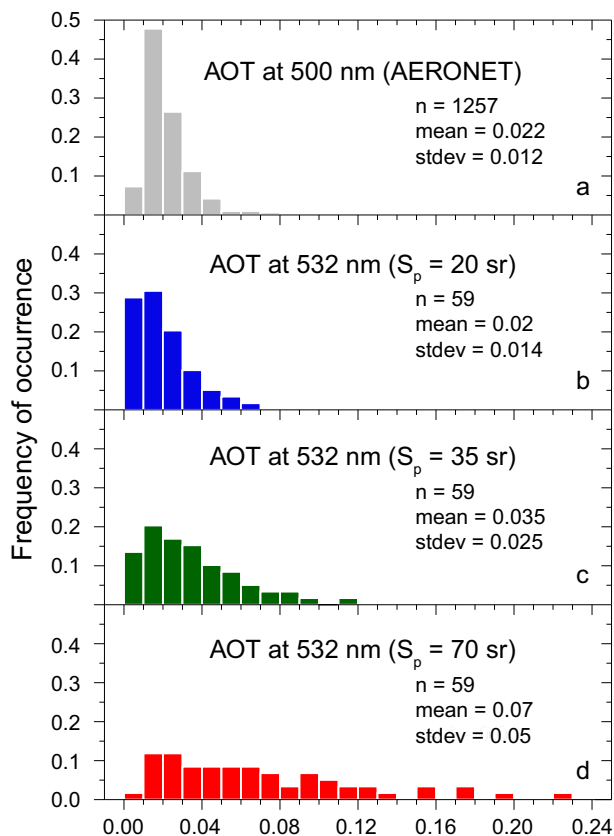


Fig. 5. Frequency of occurrence of AOT from (a) AERONET Sun photometer measurements at Rio Gallegos (level 2.0, 1257 cases), and (b–d) from Polly^{XT} measurements at Punta Arenas (59 cases) for S_p of 20, 35, and 70 sr representing clean marine, clean continental, and smoke or polluted aerosol conditions, respectively, from 4 December 2009 to 4 April 2010.

CALIPSO surface type effect on aerosol type

T. Kanitz et al.

Title Page

Abstract

Introduction

Conclusions

References

Tables

Figures

◀

▶

◀

▶

Back

Close

Full Screen / Esc

Printer-friendly Version

Interactive Discussion



CALIPSO surface type effect on aerosol type

T. Kanitz et al.

Title Page

Abstract

Introduction

Conclusions

References

Tables

Figures

◀

▶

◀

▶

Back

Close

Full Screen / Esc

Printer-friendly Version

Interactive Discussion

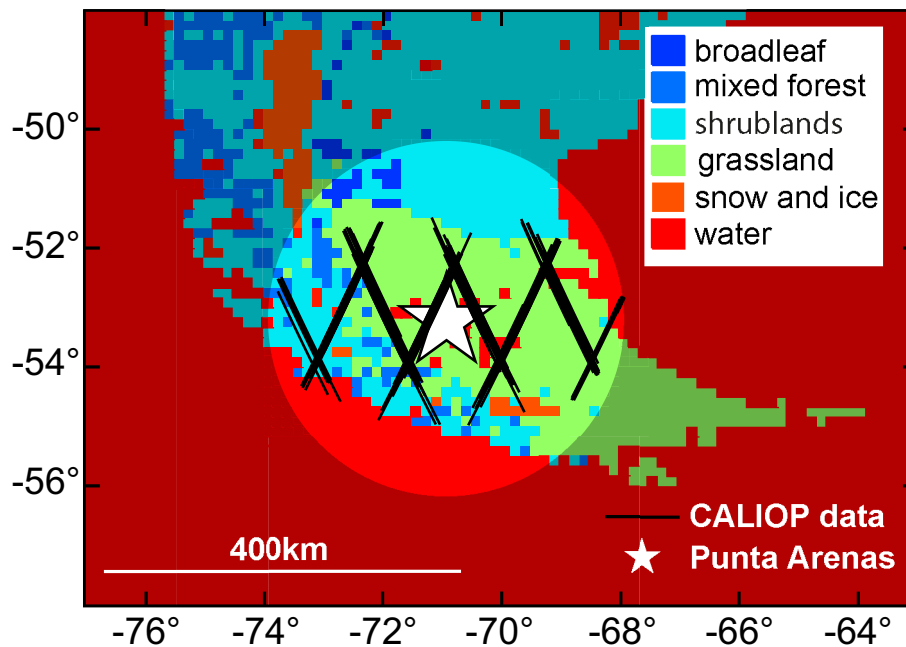


Fig. 6. International Geosphere-Biosphere Programme (IGBP, 1990) surface type map of southern Latin America and selected CALIPSO cross sections within 200 km distance of Punta Arenas.

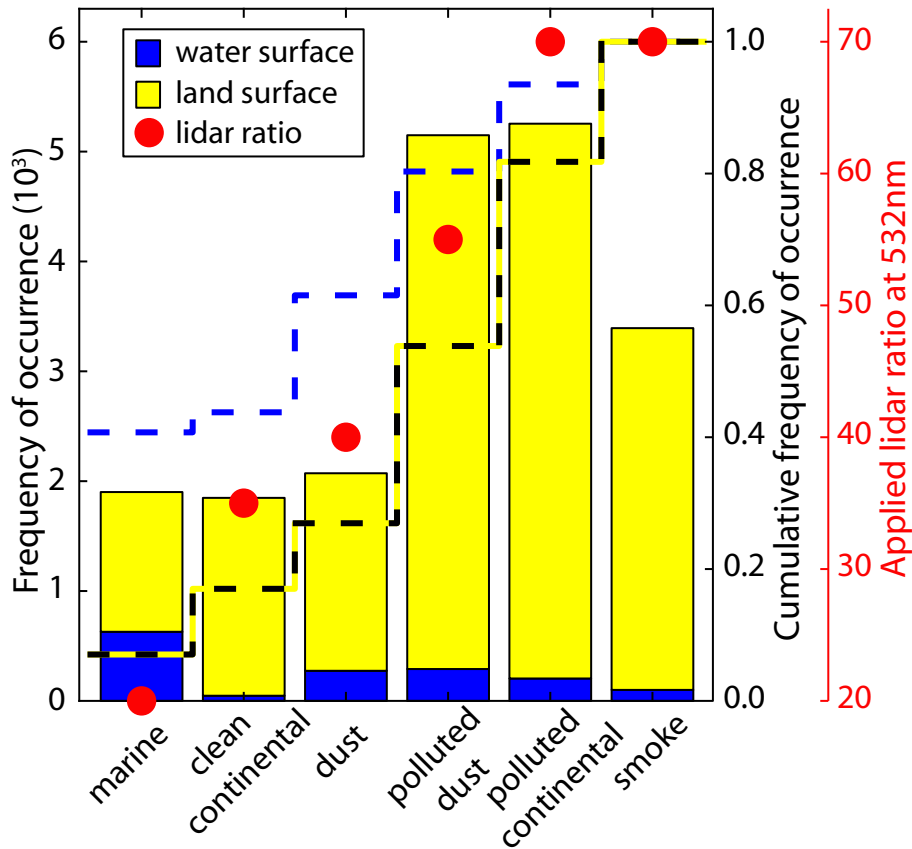


Fig. 7. Frequency of occurrence of aerosol types as determined with CALIOP from 1 May 2009 to 31 April 2010 within a distance of 200 km around Punta Arenas. Blue coloring denotes cases over water surface, yellow colors indicate cases over land surface. The cumulative frequency is given by dashed blue (water) and yellow-black lines (land). Red dots show the aerosol-type-related S_p .

CALIPSO surface type effect on aerosol type

T. Kanitz et al.

Title Page

Abstract Introduction

Conclusions References

Tables Figures

◀ ▶

◀ ▶

Back Close

Full Screen / Esc

Printer-friendly Version

Interactive Discussion



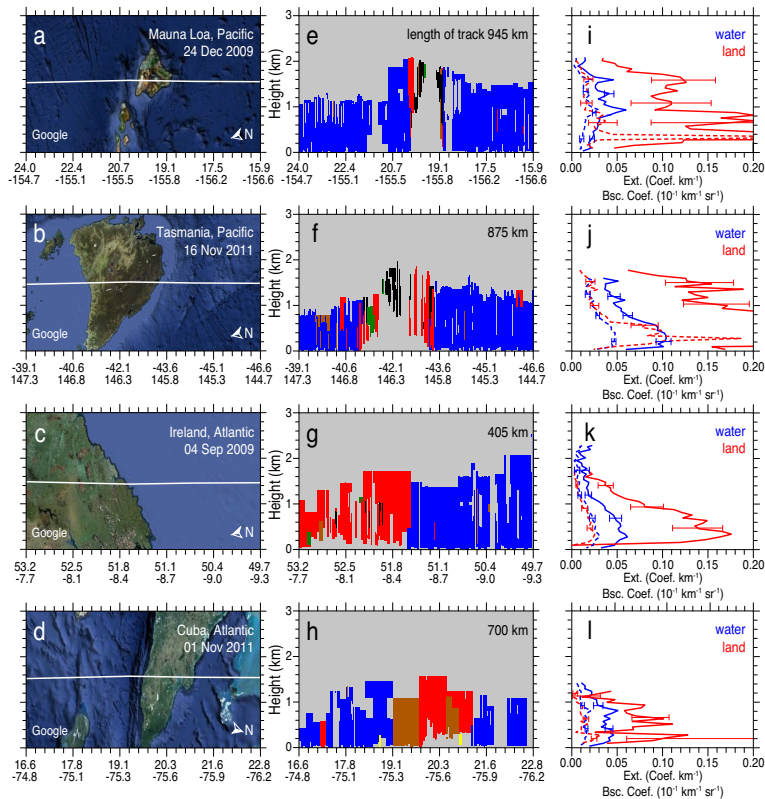


Fig. 8. (a–d) Surface type information from google Earth map of different coastal areas. Flight tracks of selected CALIPSO overflights are indicated by the white lines. Axis numbers show the coordinates of the flight track (upper row: latitude, lower row: longitude). (e–h) Height–time display of the aerosol subtype mask as determined with CALIPSO during overflight of the location to the left. The length of the selected cross section is given at the right top. (i–l) Corresponding mean profiles of 532 nm backscatter (dashed) and extinction coefficient (solid) separately for water (blue) and land surface (red).

CALIPSO surface type effect on aerosol type

T. Kanitz et al.

Title Page	
Abstract	Introduction
Conclusions	References
Tables	Figures
◀	▶
◀	▶
Back	Close
Full Screen / Esc	
Printer-friendly Version	
Interactive Discussion	



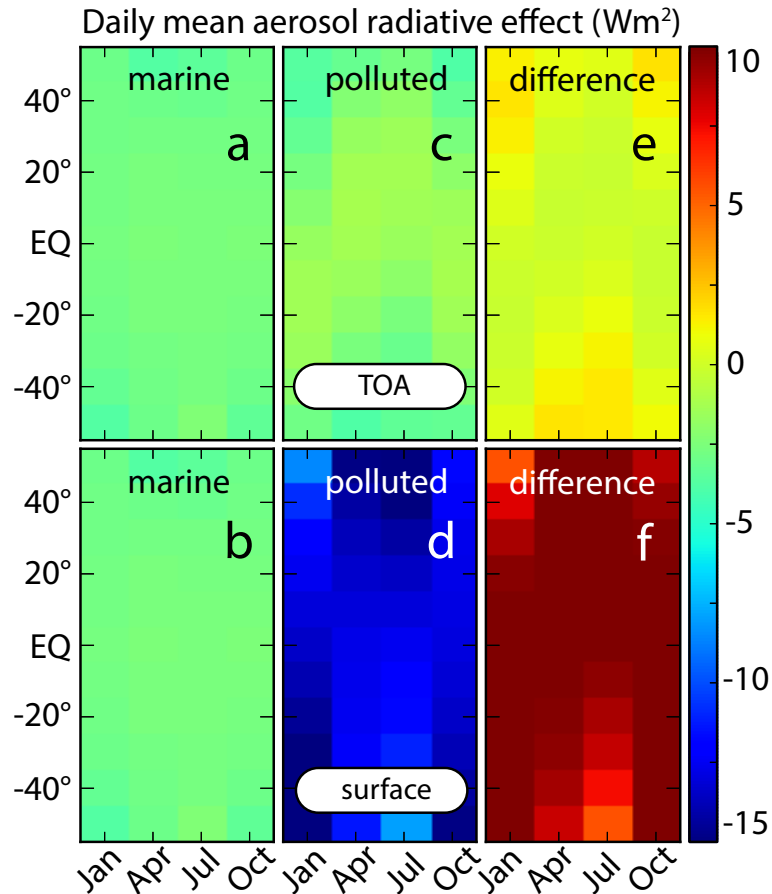


Fig. 9. Direct solar aerosol radiative effect at the top of atmosphere (TOA, top panel) and surface (bottom panel) for marine and polluted boundary-layer aerosol (left and center). Right: difference in the direct solar radiative effect of both aerosol scenarios.